

# Applications of Boron Nitride QDs

Subjects: Others

Contributor: Amit Acharya

Boron nitride quantum dots (BNQDs) have gained increasing attention for their versatile fluorescent, optoelectronic, chemical, and biochemical properties.

Keywords: Boron Nitride ; Fluorescence ; sensing ; electrochemiluminescence ; photocatalyst

## 1. Biological Application

Metal-free quantum dots such as carbon and BN quantum dots (CQDs, BNQDs) have multiple advantages over conventional semiconductor quantum dots. It is believed that CQDs and BNQDs exhibit higher photophysical, chemical, and photochemical stability. Besides, CQDs and BNQDs are non-toxic and more biocompatible [1][2]. It was reported that BNQDs are more biocompatible than carbon QDs as the latter would undesirably interact with biomolecules (DNA, proteins, or enzymes) that would compromise the intrinsic properties of these biomolecules [3]. Besides, BNQDs are more tolerant of different pH environments in the range of 2–12, with no significant effect on the fluorescence of BNQDs [4]. The cytotoxicity and biocompatibility of BNQDs were studied; excellent biocompatibility was shown [1][4][5][6][7][8][9][10][11].

### 1.1 Bioimaging

Organic dyes are popular for bioimaging applications for their relatively low cost and good biocompatibility. However, organic dyes are limited by photobleaching where their fluorescence brightness is degrading under the prolonged irradiation of excitation laser light. The use of nanoparticles such as BNQDs with strong fluorescence, photostable, nonblinking, and nonbleaching would be a good alternative for cellular imaging probes. Lin et al. have reported on the use of BNQDs for the imaging of MDCK-II (Madin-Darby canine kidney) cells by confocal microscopy in the FITC (fluorescein isothiocyanate) mode as shown in [Figure 8](#). The BNQDs were internalized into cells but did not penetrate the cell nuclei [5]. A similar study was performed on different types of cells by others [1][4][7][10][11][12]. Jung et al. [9] studied the internalization of edge-hydroxylated BNQDs (EH-BNQDs) by MCF-7 breast cancer cells and PC-3 prostate cancer cells. Blue fluorescence in the perinuclear region was demonstrated. The locations of EH-BNQDs inside the cells were compared with the locations of intracellular endosomes that were labeled with Lysotracker (red dyes), which resulted in a purple color due to the overlapping of blue and red fluorescence under confocal microscope proving the successful endocytosis of QDs. A similar study was performed on HeLa cells [4].

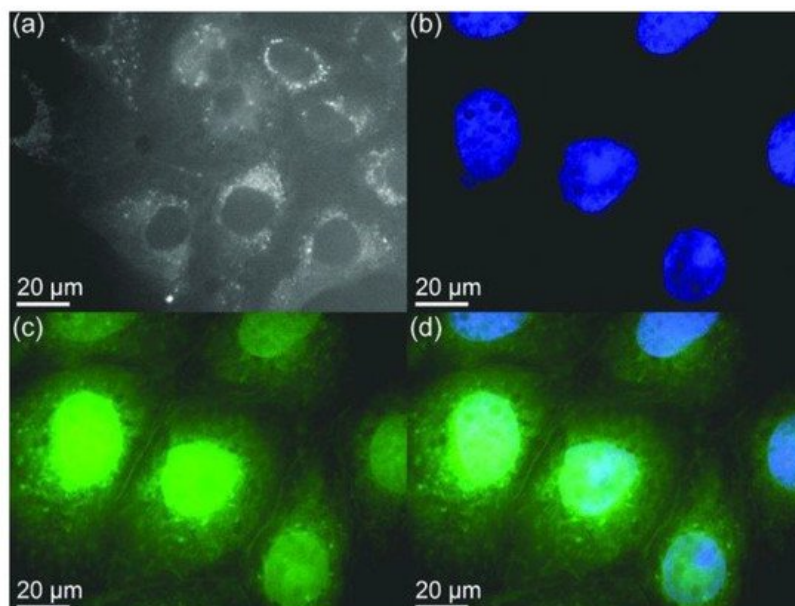


**Figure 8.** Confocal microscopy images of mammalian cells. (a) Agglomerated BNQDs surrounding each nucleus (cells are stained by BNQDs only). (b) Individual nucleus stained blue with DAPI (4', 6-diamidino-2-phenylindole). (c) BNQDs with green luminescence surrounding the nuclei. (d) The overlay image of cells stained with DAPI and BNQDs. Reproduced from [5] with permission from 2013 Wiley-VCH Verlag GmbH & Co. KGaA (Weinheim, Germany).

Thangasamy et al. [13] reported the imaging of bacterial cells (Gram-negative and Gram-positive) using BNQDs. Both types of cells were stained with 100 µg/mL of BNQDs. According to images from epi-fluorescence microscopy and confocal microscopy, the internalization of BNQDs occurred for Gram-negative cells but not for Gram-positive cells. It is to be noted that the Gram-negative cells possess an extra lipid layer outside the peptidoglycan layer, which Gram-positive cells lack. This interesting interaction of BNQDs with the outer lipid layer of Gram-negative cells can be used for Gram-negative cell identification and selective staining from environmentally mixed bacterial samples.

BNQDs exhibit a long fluorescent lifetime (FLT) and a unique excitation-dependent emission property. Therefore, BNQDs can be a good candidate for multiplex fluorescence imaging when used in conjunction with organic dyes. The combined fluorescent signals can be resolved spectrally and temporally based on the emission wavelength and the FLT, respectively. For multiple probes having overlapping emission wavelengths but different fluorescent lifetimes, both spectral and temporal imaging can be combined. Dehghani et al. [8] reported the use of two-photon excitation features of BNQDs for multiplex cell imaging. The fluorescence lifetime imaging microscopy (FLIM) was used to accurately distinguish the emission signals of BNQDs with longer FLT in comparison to relatively shorter cell autofluorescence and those from organic dyes. They reported the use of two nuclear stains: DAPI (4', 6-diamidino-2-phenylindole) with blue and Sytox with green fluorescence, both with shorter fluorescent decay lifetimes, to achieve the temporally and spectrally resolved fluorescent signals as shown in Figure 9. They co-stained the RL-14 cells with b-BNQDs/DAPI (b-BNQDs: blue-emitting BNQDs) and g-BNQD/Sytox green (g-BNQDs: green-emitting BNQDs) separately. The emission of BNQDs and dyes was not separated by spectral analysis of the image, but this issue was resolved by using the difference in fluorescence lifetimes of BNQDs and dyes using the FLIM technique.

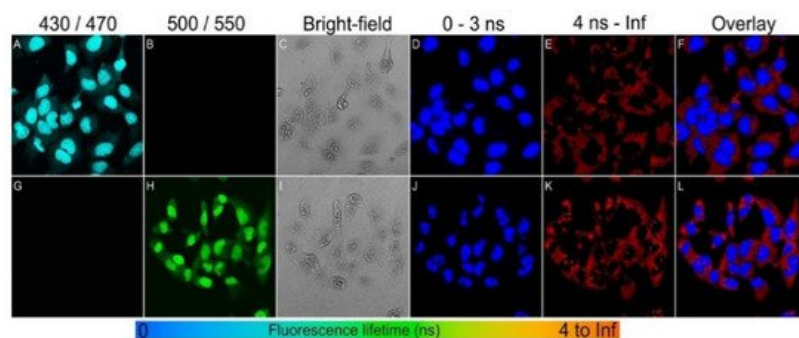


**Figure 9.** Spectral imaging (A–C,G–I) and fluorescence lifetime imaging (D–F,J–L) of RL-14 cells separately treated with b-BNQDs/DAPI and g-BNQDs/Sytox green. No emission was detected in panels B and G co-stained with QDs and stains. Fluorescence signals from b-BNQDs and g-BNQDs were resolved using spectrally matched detection ranges as seen in panels A and H. The fluorescence lifetimes were obtained by bi-exponential fitting and mapped to a false-color scale from 0 ns (blue) to >4 ns (red). The resulting false-color shows the difference between signals originating from BNQDs (panels D and J) and organic dyes (E,K). Reproduced from [8] with permission from Copyright © 2018 American Chemical Society.

## 1.2. Biosensing

Angizi et al. reported the use of BNQDs for the sensitive and selective detection of vitamin C (VC) [14]. This was performed by a modified screen-printed gold electrode (GSPE) with functionalized BNQDs. BNQDs are superior to carbon nanostructures in terms of the linear range of sensing and the detection limit. For example, a detection limit of 0.45 µM was recorded in Angizi et al.'s work while using the BNQDs/Au system, significantly lower than 3 µM for the cellulose acetate/graphite system. The high electrocatalytic activity for electro-oxidation of VC was reported and the oxidation occurred at the surface of the BN QD/Au electrode at a lower positive potential than the GSPE. Later, Jerome et al. [15] reported a rapid response sensor (1.8 sec) to detect vitamin C (ascorbic acid, AA) using BNQDs and polyluminal (Plu) coated glassy carbon electrode (GCE). As-prepared hybrid Plu/BNQDs coated GCE was reported to show improved electrocatalytic activity for AA oxidation at 0.2 V using the amperometry detection method. Further, they carried out the interference effects in the presence of uric acid, dopamine, and glucose which did not respond to the Plu/BNQDs/GCE sensors, indicating good selectivity of the sensor for AA. In another study, Kong et al. [16] reported a fluorescent “on-off-on” sensor to detect AA with Fe<sup>3+</sup> as a medium. The fluorescence of BNQDs was quenched due to the inner filter effect between Fe<sup>3+</sup> and BNQDs. Then, the fluorescence of BNQDs was restored with increasing AA due to the oxidation-reduction between Fe<sup>3+</sup> and AA. This technique enabled the detection of AA in the concentration range 1–100 µM with a

detection limit of 0.0833  $\mu\text{M}$  under the optimized experimental conditions at pH 6. The sensing selectivity of BNQDs to  $\text{Fe}^{3+}$  ions was confirmed by comparing data obtained by using other metal ions. Other metal ions had a negligible effect on quenching BNQD fluorescence. The selectivity of BNQDs on AA sensing was also verified by replacing AA with other interfering substances, such as uric acid, dopamine, and glucose. These substances have shown little recovering effect on the fluorescence of BNQDs. All these data support the fact that BNQDs exhibit high selectivity for  $\text{Fe}^{3+}$  and AA.

Dehghani et al. [18] reported the use of g-BNQDs passivated with polyethylene glycol, for the biosensing of intracellular pH variations and their distribution inside cells. This was performed by confocal microscopy and FLIM techniques. It is to be noted that the increase in incubation time will cause the micro-environment of the cells to become more acidic due to the formation of more endosomes. The acidic environment would result in a shorter FLT. The authors reported the translocation and accumulation of g-BNQDs at endosomes over 4 h, which resulted in the change of cell morphology. The quenching of photoluminescence of BNQDs in an acidic medium can be utilized for detecting changes in metabolic activity inside human cells. Owing to the Warburg effect [17], lactate production in cancer cells during glycolysis is high. Therefore, the extracellular pH of tumor cells is often acidic, leading to a high extracellular acidification rate (ECAR) compared to benign cells. Radhakrishnan et al. [19] reported the use of the glycolytic inhibitor, 3-bromopyruvate(3-BP), to suppress ECAR. This was demonstrated by monitoring the increase in fluorescence from FBNQDs, as a method to detect the glycolytic activity in cancer cells. In this case, the green fluorescence channel of flow cytometry was used to detect the enhanced fluorescent signal after introducing 3-BP to cancer cells. There was no considerable change in fluorescence in benign cells due to a less active glycolytic pathway. In another study, Yola et al. [19] reported a stable, repeatable, reusable, and selective imprinted biosensor based on BNQDs for cardiac Troponin-I (cTnI) detection in plasma samples. The cTnI is widely used for the diagnosis of acute myocardial infarction (AMI) diseases. Later, the same group [20] reported the preparation of a novel voltammetry sensor for the detection of various organophosphate pesticides in water samples based on BNQDs on graphene oxide.

Owing to the strong inner filter effect between 2,4,6-trinitrophenol (TNP) and BNQDs, the fluorescence intensity of BNQDs can be reduced upon quenching by TNP. By this mean, TNP can be selectively and sensitively detected in the concentration range of 0.25–200  $\mu\text{M}$ , with a detection limit of 0.14  $\mu\text{M}$  when BNQDs are used as fluorescence probes [21]. Therefore, BNQDs can be used as the turn-off sensors for the rapid detection of TNP from natural water sources without tedious pretreatment processes. Similarly, Peng et al. [22] reported a “switch on” nanosensor for sensitive assay of glutathione (GSH). GSH can regulate the inner filter effect of  $\text{MnO}_2$  nanosheets (NS) on BNQDs. Owing to the superior light absorption capability of redox-able  $\text{MnO}_2$ NS centered at 380 nm, the fluorescence of BNQDs (with a maximum emission wavelength 380 nm) can be selectively quenched. For an optimal inner filter effect to take place between the two substances, the maximum absorption of one should overlap the maximum emission of the other. However, the introduction of GSH will help to recover the fluorescence of BNQDs, dependent on the concentration of GSH, by weakening the inner filter effect as initiated by the decomposition of  $\text{MnO}_2$  to  $\text{Mn}^{2+}$ . This  $\text{MnO}_2$ NS/BNQDs nanoprobe was reported to exhibit good selectivity on GSH detection in the range of 0.5–250  $\mu\text{M}$  with a detection limit of 160 nm in human plasma samples. They reported the use of other interference substances such as histidine, glutamic acid, cysteine, vitamin C, sodium chloride, potassium chloride, etc., instead of GSH in the same concentration which did not show much change in fluorescence recovery, thus suggesting the need for the separation of interfering reductants from real samples. The sensing principle is shown in [Figure 10](#).

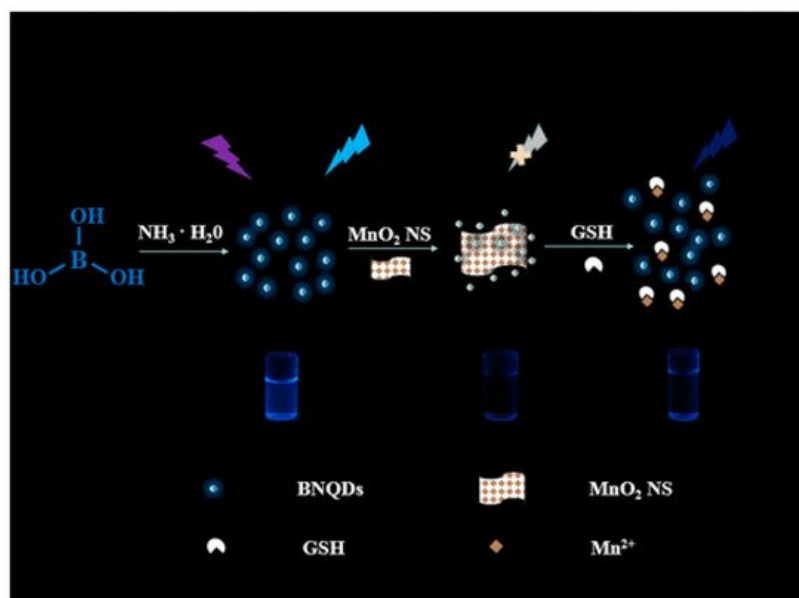


**Figure 10.** Schematic principle of glutathione (GSH) regulated IFE (inner filter effect) of  $\text{MnO}_2\text{NS}$  on BNQDs for sensing. The observed fluorescence of BNQDs is quenched with the  $\text{MnO}_2\text{NS}$  presence and later recovered with GSH application. Reproduced from [22] with permission from copyright © 2019 American Chemical Society.

In addition to the inner filter effect, fluorescence resonance energy transfer (FRET) on BNQDs also offers interesting application. For example, FRET between BNQDs and gold nanoparticles (AuNPs) has enabled the fabrication of rapid, label-free, and highly sensitive fluorescence-based biosensors [23]. Such sensors were used to detect acetylcholinesterase (AChE), a key enzyme in the biological nerve conduction system, whose activities have been connected to several diseases such as muscular paralysis, convulsions, and bronchial constriction. As reported, AChE can hydrolyze acetylthiocholine (ATCh) to generate thiocholine (TCh) whose thiol (-SH) group can reduce chloroauric acid ( $\text{HAuCl}_4$ ) to AuNPs. The formation of TCh-BNQDs/AuNPs aggregates can quench the fluorescence of BNQDs via FRET. An inhibitor, paraoxon, was used to lower the activity of AChE and decreased the fluorescence quenching of BNQDs. In this way, a simple 'one-pot' FRET-based biosensor was reported to be constructed to assess AChE activity and its inhibitor by analyzing the fluorescence of BNQDs.

## 2. Chemical Sensing

Liu et al. reported the use of BNQDs as fluorescence probes to determine the concentration of ferrous ( $\text{Fe}^{2+}$ ) and ferric ( $\text{Fe}^{3+}$ ) ions with high selectivity, sensitivity, and a low detection limit [24]. For this study, the change in fluorescence intensity with various concentrations of ions (10–600  $\mu\text{M}$ ) was investigated at the excitation wavelength of 310 nm. Gradual quenching with increasing concentration resulting in lower fluorescence intensity due to electron transfer from BNQDs to  $\text{Fe}^{2+}$  and  $\text{Fe}^{3+}$  ions was reported as seen in Figure 11. The PL quenching efficiency at excitation wavelength 310 nm at various ions concentration showed two linear trends (one for a concentration range of 0–250  $\mu\text{M}$ , and another one for the range of 300–650  $\mu\text{M}$ ) for both types of ions. Though the total concentration of both ions can be determined regardless of the oxidation states, detecting individual ions from the mixture is still challenging using this procedure. A similar study for  $\text{Fe}^{3+}$  detection was reported by Kong et al. [16].

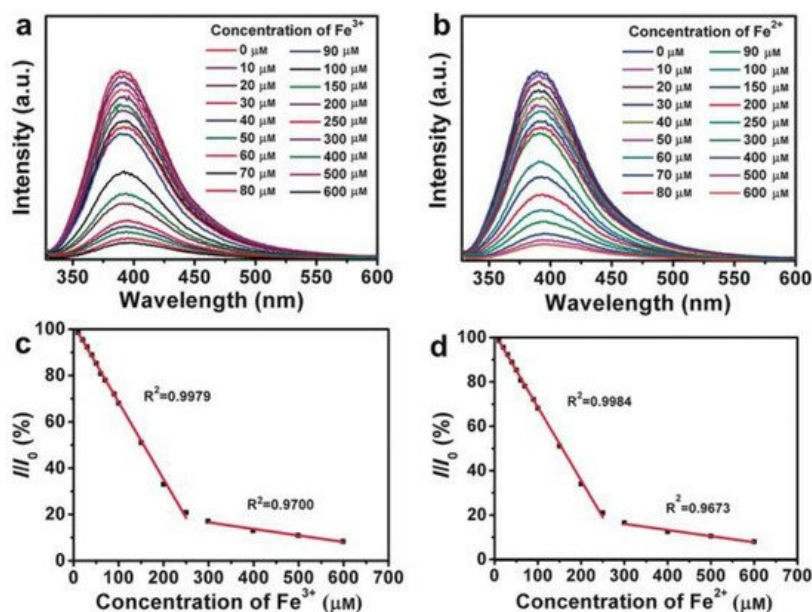


**Figure 11.** BNQDs-based sensing of (a)  $\text{Fe}^{3+}$  and (b)  $\text{Fe}^{2+}$  by measuring the PL intensity at  $\lambda_{\text{ex}} = 310$  nm, with ion concentrations of 10, 20, 30, 40, 50, 60, 70, 80, 90, 100, 150, 200, 250, 300, 400, 500, and 600  $\mu\text{M}$ , and the linear relationship between the PL-quenching efficiency ( $I/I_0$ ) at  $\lambda_{\text{ex}} = 310$  nm and the concentration of (c)  $\text{Fe}^{3+}$  and (d)  $\text{Fe}^{2+}$ . Reproduced from [24] with permission from copyright © 2016 Wiley-VCH Verlag GmbH & Co. KGaA (Weinheim, Germany).

Nickel ( $\text{Ni}^{2+}$ ) ions were reported to be detected in natural water samples via quenching of the fluorescence of BNQDs [25]. Liu et al. reported that the BNQDs prepared in *N*-methyl-2-pyrrolidone (NMP) with green fluorescence were much more competitive than those prepared in ethanol and DMF with blue fluorescence as a competitive fluorescent sensing probe for label-free specific detection of  $\text{Fe}^{3+}$  or  $\text{Cu}^{2+}$  [4].

Huo et al. [3] reported the strongest fluorescence quenching phenomenon for BNQDs dispersion with  $\text{Fe}^{3+}$  ions due to the aggregation of BNQDs. There was no obvious fluorescence emission quenching due to other metal ions of the same concentration. This makes BNQDs unique as a selective fluorescence sensing agent for  $\text{Fe}^{3+}$  ions. In addition to  $\text{Fe}^{3+}$  ion detection in DI (deionized) water, Dehghani et al. [8] explored the intracellular  $\text{Fe}^{3+}$  ions detection with the help of non-

passivated blue-emitting BNQDs (b-BNQDs). The intercellular detection limit for  $\text{Fe}^{3+}$  ions was reported as 20.6 nM, which is among the highest sensitivity reported to date. Further, Han et al. [26] reported the fluorescence quenching of BNQDs using  $\text{Fe}^{3+}$  and  $\text{Cu}^{2+}$  ions. Interestingly, the fluorescence signals can be switched on and off upon the addition of pyrophosphate (PPi) and alkaline phosphatase (ALP), respectively. The specific detection of PPi and ALP was achievable based on the switch-on and switch-off states of the fluorescence of BNQDs. By comparison of the percentage of fluorescence quenching and recovery of BNQDs, 300  $\mu\text{M}$   $\text{Fe}^{3+}$ -mediated fluorescence quenching was found to be more efficient for the sensitive and selective sensing of ALP. The ALP activity measurement was achieved in a linear range between 2 and 200  $\text{U L}^{-1}$  with a low limit of detection of 0.8  $\text{U L}^{-1}$ . Recently, Yang et al. [27] reported an efficient method to determine tetracyclines (TCs) using ratiometric fluorescence sensors based on BNQDs and europium ion ( $\text{Eu}^{3+}$ ) systems. This system worked as a probe that detected the quenching of blue fluorescence of BNQDs when introduced with TCs, while enhancing the red fluorescence of  $\text{Eu}^{3+}$ . This phenomenon can be attributed to the inner filter effect, photo-induced electron transfer, and antenna effect. The authors also reported the use of this sensor in the quantitative detection of TCs in milk and beef samples with acceptable recoveries. Further, they developed a test paper for the visual detection of TCs demonstrating the sensor practical application.

### 3. Gas Sensing

Gas sensor fabrication based on BNQDs' decorated zinc oxide (ZnO) nanoplates was reported by Choudhury et al. [28]. These sensors were used for sensing benzene, toluene, ethyl benzene, and xylene (BTEX) vapors. Sensitive sensing of these vapors is important as they are highly toxic and carcinogenic. The sensing response of these ZnO-BNQDs was enhanced greatly as compared to pure ZnO. The X-ray Photoelectron Spectroscopy (XPS) study on this BNQDs-ZnO composite showed that BNQDs are electrically interacted with ZnO via the oxygen atoms and acted as the catalysts for generating charge carriers. The increase in the number of oxygen species decides the sensing capabilities of the composites. This resistance-based gas sensor is based on the variation of conductance resulting from the chemisorption of oxygen molecules on the surface of the sensor. When the gas molecules of BTEX are adsorbed on the sensor surface, they react with the ionized oxygen and lead to oxidation decomposition of BTEX molecules, resulting in electron transfer to the sensor. An optimal temperature of 370  $^{\circ}\text{C}$  was used for the concentration-dependent studies. The response and recovery time of the sensor were reported within 20 s and had good stability.

### 4. Temperature Sensing

Li et al. utilize the variation of PL spectrum intensities of BNQDs with the temperature change as the working principle of temperature sensors [29]. They reported that PL intensities decrease linearly with the increase in temperature from 80 to 440 K when excited at 394 nm, thus making portable non-contact temperature sensors by using BNQDs. The decrease in PL intensity with the increase in temperature is due to the increase in the thermally active nonradiative relaxation process. The PL intensity is reported to be thermally activated with an activation energy of 83.9 meV and has good reversibility. The authors also reported the effect of the size of BNQDs on the sensitivity of the sensor. The relative sensitivity of the sensor with 17.7 nm BNQDs reached the maximum of 0.45 %  $\text{K}^{-1}$  at 440 K as compared to 0.73%  $\text{K}^{-1}$  at 440 K with 4.6 nm BNQDs. The relative sensitivity of the sensor based on 4.6 nm BNQDs is better than other materials such as Manganese (Mn), Zinc oxide (ZnO), Erbium (Er), and Ytterbium (Yb)-based sensors reported so far [30][31][32]. Besides, the sensors based on BNQDs exhibit the widest temperature detection range as compared with other noncontact temperature sensors based on silver nanoclusters, cadmium telluride (CdTe), Zinc sulfide (ZnS), and carbon QDs, as reported in [33][34][35][36][37].

### 5. Fluorescent Staining

Cotton fibers stained with BNQDs were reported to show the excitation wavelength-dependent fluorescence. These fibers emit green and red fluorescence when exposed to blue (450–480 nm) and green (510–550 nm) excitation light, respectively, as shown in Figure 12. This work demonstrated that BNQDs are potential fluorochromes for chemical staining [3]. A similar study was reported later on cotton and silk fibers [4].

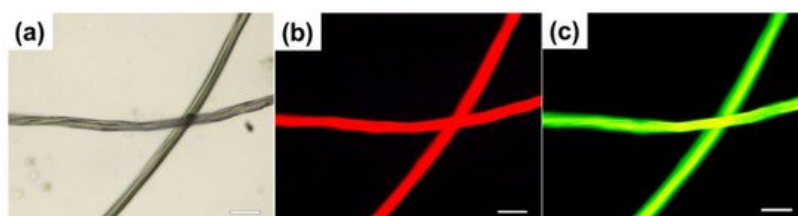


**Figure 12.** (a) Bright-field image of cotton fibers stained with BNQDs. (b) Fluorescence image of cotton fibers stained with BNQDs obtained at the excitation wavelengths of 510–550 nm. (c) Fluorescence image of cotton fibers stained with BNQDs obtained at the excitation wavelengths of 450–480 nm. Scale bar: 50  $\mu\text{m}$ . Reproduced from [3] with permission from copyright © 2017 American Chemical Society.

## 6. Electrochemiluminescence (ECL) Responses

ECL is luminescence produced by the electrochemical process where a species generated at the electrodes undergo electron transfer reactions to form excited states and emit light. This is a means to convert electrical energy into light energy without the use of excitation light. The ECL mechanism could enable an analytical tool for clinical detection. For example, the ECL of Ruthenium(II) Tris(2,2'-bipyridyl) ( $\text{Ru}(\text{bpy})_3^{2+}$ ) and its derivatives-based was demonstrated with excellent efficiency [38]. ECL was also applied in commercial instruments for immunoassays and DNA analyses with high sensitivity and selectivity [39]. For enhanced ECL performance, a suitable co-reactant is needed.

BNQDs, having excellent chemical inertness, exhibit low toxicity and can be used as the alternative ECL luminophores. The ECL property of BNQDs was first reported by Liu et al. [4] using L-cysteine (RSH) as a co-reactant. As shown in Figure 13A, BNQDs displayed ECL emission at an electrode potential of  $-1.91\text{ V}$ . Adding RSH as the co-reactant, the ECL intensity increased almost five times. ECL was not detected with RSH alone without BNQDs. The reported ECL mechanism is illustrated in Figure 13B. As shown, oxidation of RSH produces free radical intermediates including RS,  $\text{RSO}$ ,  $\text{RSO}_2$ , and  $\text{RSO}_3$ , which reacted with the electron-rich BNQDs (electron transferred from Pt electrode to BNQDs). BNQDs were excited after such electron transfers and emitted measurable luminescent signals. The effect of buffer pH on the ECL behavior was reported. It was shown that the ECL intensity increase with the increase in the buffer pH from 3 to 7, and then decreases when the pH increased over 7, as summarized in Figure 13C. Figure 13D shows the ECL emission of BNQDs with RSH under continuous 14 cyclic voltametric sweeping with good repeatedly [4].

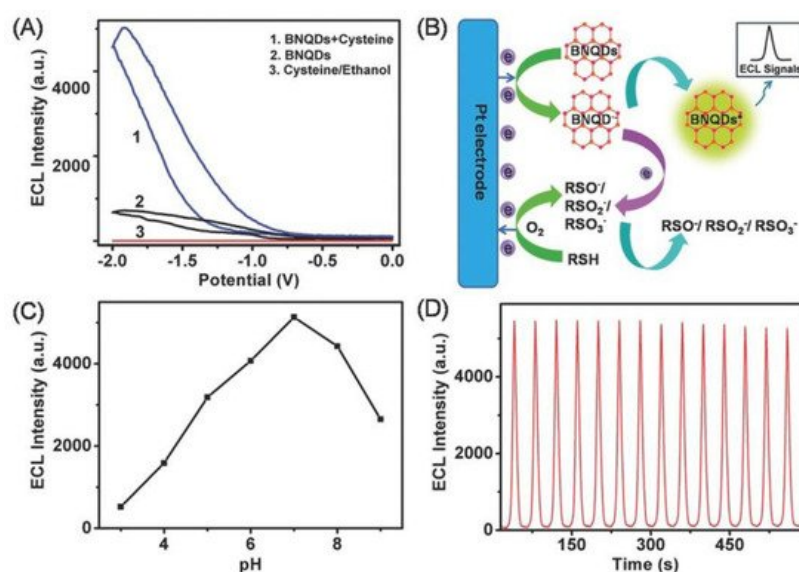


**Figure 13.** (A) Electrochemiluminescence (ECL) intensity–potential curves of  $100\text{ mg mL}^{-1}$  BNQDs prepared in ethanol in  $100 \times 10^{-3}\text{ m}$  PBS (pH 7.0) with varying condition. (B) Schematic illustration of the ECL mechanism of the BNQDs/L-cysteine (RSH) system. (C) Influences of buffer pH on the ECL intensity of  $100\text{ mg mL}^{-1}$  BNQDs. (D) ECL intensity–time curve under continuous cyclic voltammetry scanning between  $-2.0$  and  $0\text{ V}$  for  $600\text{ s}$  for the BNQDs/RSH system. The scan rate is  $100\text{ mV s}^{-1}$ . Reproduced from [4] with permission from 2016 Wiley-VCH Verlag GmbH & Co. KGaA (Weinheim, Germany).

Later, Xing et al. [40] reported an enhanced and stable anodic ECL from a suspension of BNQDs and  $\text{Ru}(\text{bpy})_3^{2+}$ , which had a 400-fold enhancement compared with individual  $\text{Ru}(\text{bpy})_3^{2+}$ . BNQDs functionalized with amino groups and the electrocatalytic effect made them efficient co-reactants of  $\text{Ru}(\text{bpy})_3^{2+}$ . The effect of atmosphere and electrode materials on ECL performance was reported. For example, ECL intensity under saturated nitrogen was reported to be higher than that obtained in the air and oxygen atmosphere. The use of glassy carbon electrode yielded better ECL intensity as compared with gold and platinum electrodes. Although tripropylamine (TPA) was shown to be the better co-reactant, BNQDs are the better choice for their better solubility, chemical stability, biocompatibility, and ease of synthesis. Further, ECL sensing for dopamine (DA) was reported based on the quenching effect between the excited state of  $\text{Ru}(\text{bpy})_3^{2+}$  and the oxidation form of DA in the ECL system of  $\text{Ru}(\text{bpy})_3^{2+}$ /BNQDs [40]. In another study, BNQDs were used as the co-reactants in label-free ECL immune-sensors. Such sensors are based on antigen–antibody interaction for alpha-

fetoprotein (AFP) detection in human serum as reported by Qin et al. [41]. The authors integrated Ru(bpy)<sub>3</sub><sup>2+</sup>-doped silica nanoparticles (Ru-SiO<sub>2</sub>) and AuNP-modified graphene oxide (rGO@Au) to form a rGO@Au@Ru-SiO<sub>2</sub> composite which was used as the ECL probe of the sensors. The anode ECL intensity of this composite on GCE was low, but the addition of BNQDs enhanced the ECL intensity by about 100 times. The ECL immuno-sensor was applied for quantitative detection of AFP antigen as ECL signal decreased with the increase in AFP concentration from 0.0001 to 100 ng mL<sup>-1</sup>. This immune sensor exhibited a low detection limit, high selectivity and sensitivity, acceptable stability, and a wide linear detection range.

The emission spectrum of BNQDs is perfectly matched with the absorption spectrum of nitrogen-doped graphene QDs (NGQDs). Based on this property, Li et al. have demonstrated folic acid (FA) sensors with good selectivity and high recoveries based on ECL resonance energy transfer (ECL-RET) between BNQDs and NGQDs in the presence of co-reactant K<sub>2</sub>S<sub>2</sub>O<sub>8</sub> [42]. The intermediate state of K<sub>2</sub>S<sub>2</sub>O<sub>8</sub>, SO<sub>4</sub><sup>2-</sup>, oxidizes FA and decreases the NGQDs/BNQDs/K<sub>2</sub>S<sub>2</sub>O<sub>8</sub> ECL signal, resulting in the signal-off detection of FA. The ECL intensity of NGQDs by RET was improved by about 10-fold by the addition of BNQDs. This reported method has an advantage against other reported ECL-RET-based sensors [43][44][45][46] that use toxic heavy metal QDs that cause serious health and environmental concerns.

Another study by Liu et al. demonstrated the use of BNQDs and gold nanoparticles (AuNPs) as biosensors to accurately quantify the Shiga toxin-producing Escherichia Coli gene from 1 pmol L<sup>-1</sup> to 5 nmol L<sup>-1</sup> with a limit of detection of 0.3 pmol L<sup>-1</sup> [47]. This biosensor can be used for DNA detection and was designed based on the ECL-RET principle, and surface plasmon coupling (SPC) effects between AuNPs and BNQDs. In brief, a hairpin DNA probe was made by binding BNQDs and AuNPs to its end. The ECL signal of the BNQDs was quenched by the AuNPs due to ECL-RET between the AuNPs and BNQDs. When the hairpin DNA probe identified the target DNA, the distance between BNQDs and AuNPs increased due to the linear transformation of the hairpin structure. As a result, the SPC-ECL effect suppressed the ECL-RET effect, thus enhancing the ECL signal (due to coupling of light emission with surface plasmon resonance) by about six times higher than BNQDs-Au NPs- hairpin DNA conjugates. The authors further reported on the use of S-regulated BNQDs along with AuNPs with higher ECL performance for BRAF gene detection and quantification using the same SPC-ECL strategy as discussed above [48]. Further, Liang et al. [49] reported the first polarized-ECL biosensor developed using SPC-ECL strategy and fluorine-doped BNQDs to detect the K-ras gene. The fluorine-doped BNQDs ECL signal was reported to be enhanced at a specific polarization angle, thanks to polarization angle-dependent SPC-ECL. This polarized-biosensor was reported to quantify the K-ras gene from 0.1 fM to 10 nM, with the detection limit as 0.03 fM.

Recently, Wang et al. [50] reported the construction of ECL biosensor using BNQDs as a co-reactant of luminol for the quantitative determination of concanavalin A (Con A). BNQDs are used for boosting the ECL intensity of luminol, almost producing a 10-fold enhancement as compared with single poly (luminol/aniline) nanorods loaded on reduced graphene oxide using GCE. The detection limit of Con A was reported in the range of 1.0 pgmL<sup>-1</sup> to 1.0 μgmL<sup>-1</sup> with a low detection limit of 0.15 pgmL<sup>-1</sup>.

## 7. Photocatalyst

Radhakrishnan et al. reported the use of TiO<sub>2</sub> nanotubes/FBNQDs heterojunctions as the broad-spectrum photocatalyst for efficient water splitting [18]. Hydrogen production enhancement was reported when FBNQDs were loaded on TiO<sub>2</sub> nanotubes (NT). This was demonstrated by using photoelectrochemical cells consisting of the platinum cathode, and TiO<sub>2</sub> nanotubes/FBNQDs photoanode, where visible light from solar radiation was used to generate hydrogen and oxygen from water. A hydrogen production conversion efficiency of up to 24% was obtained after adding FBNQDs onto TiO<sub>2</sub> nanotubes, paving an alternative way in the design of efficient visible-light photocatalysts. Later, Yang et al. reported metal-free heterostructure photocatalyst using ultrathin porous graphitic carbon nitride (UPCN) decorated with BNQDs [51]. The use of BNQDs has promoted the dissociation of excitons and accelerated the transfer of charges. This BNQDs/UPCN (BU) photocatalyst used visible light to degrade oxytetracycline hydrochloride (OTC-HCl) for molecular oxygen activation by the generation of superoxide radical (O<sub>2</sub><sup>-</sup>). Further, BU photocatalyst along with visible light irradiation was used to produce hydrogen peroxide (H<sub>2</sub>O<sub>2</sub>) from the mixture of IPA and deionized water. The average O<sub>2</sub><sup>-</sup> generation rate for the best-optimized sample was about 2.3 and 1.6 times better than that of bulk graphitic carbon nitride (g-C<sub>3</sub>N<sub>4</sub>) and UPCN, respectively. Moreover, the H<sub>2</sub>O<sub>2</sub> production by the same sample was 3.2 and 2 times higher than that of bulk g-C<sub>3</sub>N<sub>4</sub> and UPCN, respectively, for 60 min.

The incorporation of BNQDs to tungsten trioxide (WO<sub>3</sub>) photoanode was reported for efficient photogenerated charge separation, and charge recombination for the photoelectrochemical (PEC) water splitting application [52]. It was thought that BNQDs help to extract the photogenerated holes, thus enhancing charge separation and water oxidation potency. A 2.4-fold enhancement in photocurrent density and 2.44-fold enhancement in charge carrier density were reported by using

such BNQD-modified photoanode in comparison to the pristine  $\text{WO}_3$  anode. Moreover, the incident photon to current conversion efficiency (IPCE) using the modified photoanode has reached 32%, which is 2.1 times higher than that when pristine  $\text{WO}_3$  anode was used. On the other hand, Sahu et al. reported superior PEC performance in water splitting using BNQDs incorporated over fluorine-doped hematite ( $\text{F-Fe}_2\text{O}_3$ ) nanorods [53]. 1-D hematite nanorod arrays quickly transferred electrons to the FTO substrate, while BNQDs acted as the efficient hole extractors that enhanced charge separation on the hematite surface by decreasing the hole trapping probability. In the optimal condition, a carrier density of  $2.08 \times 10^{20} \text{ cm}^{-3}$  was obtained, which is two orders of magnitude higher than that when bare  $\alpha\text{-Fe}_2\text{O}_3$  photoanode was used. This resulted in a photocurrent density of  $2.24 \text{ mA cm}^{-2}$  at 1.23 V, which is six-fold higher than the case when bare hematite was used. The faradaic efficiency test of  $\text{F-Fe}_2\text{O}_3$ -BNQDs for oxygen evolution was reported to be 90% after 1 h of irradiation, confirming that most of the photo-generated charges were utilized for water oxidation.

## 8. Other Applications

Because of the low shielding effect of the h-BN planes in proton transport [54], BNQDs suspended in water were investigated for their roles in proton exchange membranes (PEMs) by Lei et al. [1]. The authors reported easy integration of BNQDs into polymer matrix resulting in enhanced thermal stability and proton conductivities of the composite PEMs with an enhanced water retention capability.

With the electronic devices getting smaller and smaller with high integration and power density, dissipating heat effectively is highly desirable for ensuring their long lifetime and reliability. The good thermal conductivity and excellent electrical insulation in h-BN materials make them a good candidate for thermal management applications. BN nanosheets were added into the polymer matrix as filler to form effective thermal conductive paths that significantly improve the thermal conductivity of the composites [55][56][57][58][59][60][61][62]. Theoretical studies on thermoelectric properties of BNQDs were conducted to inspire experimentalists to seek ways for real-world applications [63]. For example, Zhou et al. [64] reported the doping of BNQDs on a flexible polyamide-imide (PAI)/BN nanosheets composite film to improve the thermal conductivity (TC) of the polymer and track the thermal conductive paths utilizing the photoluminescence (PL) of BNQDs. In this case, BNQDs were filled into the gaps between the BN nanosheet fillers and the polymer matrix, forming the continuous thermal conductive paths. For low filler content (BN nanosheets 9% wt) and 1% wt BNQDs, the hybrid composite film resulted in an in-plane TC of  $7.69 \text{ W m}^{-1} \text{ K}^{-1}$  and had good optical transparency, making it a possible candidate for use as a flexible display substrate.

The use of BNQDs as readout labels for logic gate construction was first reported by Han et al. [26] based on the principle of signal-on and-off in the BNQDs- $\text{Fe}^{3+}$  FL in the PPI and ALP assays. The existence of PPI and ALP was used as the inputs ("1" state for present and "0" state for absence). The normalized FL intensity of BNQDs under optimal excitation conditions was used as the output signal. The reported application for inhibiting "INH" logic gate construction could pave a path for the use of other 2D-QDs for a future logic gate design.

Beytur [65] reported the use of BNQDs in preparation for Platinum nanoparticle (PtNPs)/BNQDs/6-methyl-2-(3-hydroxy-4-methoxybenzylideneamino)-benzothiazole(ILs)nanocomposite (PtNPs/BNQDs/ILs) for the electrocatalytic oxidation of methanol. The performance of this nanocomposite was better than while using only ILs and BNQDs/ILs.

---

## References

1. Lei, Z.; Xu, S.; Wan, J.; Wu, P. Facile preparation and multifunctional applications of boron nitride quantum dots. *Nanoscale* 2015, 7, 18902–18907.
2. Lim, S.Y.; Shen, W.; Gao, Z. Carbon quantum dots and their applications. *Chem. Soc. Rev.* 2015, 44, 362–381.
3. Huo, B.; Liu, B.; Chen, T.; Cui, L.; Xu, G.; Liu, M.; Liu, J. One step synthesis of fluorescent boron nitride quantum dots via a hydrothermal strategy using melamine as nitrogen source for the detection of ferric ions. *Langmuir* 2017, 33, 10673–10678.
4. Liu, M.; Xu, Y.; Wang, Y.; Chen, X.; Ji, X.; Niu, F.; Song, Z.; Liu, J. Boron nitride quantum dots with solvent-regulated blue/green photoluminescence and electrochemiluminescent behavior for versatile applications. *Adv. Opt. Mater.* 2017, 5, 1600661.
5. Lin, L.; Xu, Y.; Zhang, S.; Ross, I.M.; Ong, A.C.M.; Allwood, D.A. Fabrication and luminescence of monolayered boron nitride quantum dots. *Small* 2013, 10, 60–65.
6. Li, H.; Tay, R.Y.; Tsang, S.H.; Zhen, X.; Teo, E.H.T. Controllable synthesis of highly luminescent boron nitride quantum dots. *Small* 2015, 11, 6491–6499.

7. Xue, Q.; Zhang, H.; Zhu, M.; Wang, Z.; Pei, Z.; Huang, Y.; Song, X.; Zeng, H.; Zhi, C. Hydrothermal synthesis of blue-fluorescent monolayer BN and BCNO quantum dots for bio-imaging probes. *RSC Adv.* 2016, 6, 79090–79094.
8. Dehghani, A.; Ardekani, S.M.; Lesani, P.; Hassan, M.; Gomes, V.G. Two-photon active boron nitride quantum dots for multiplexed imaging, intracellular ferric ion biosensing, and pH tracking in living cells. *ACS Appl. Bio Mater.* 2018, 1, 975–984.
9. Jung, J.-H.; Kotal, M.; Jang, M.-H.; Lee, J.; Cho, Y.-H.; Kim, W.-J.; Oh, I.-K. Defect engineering route to boron nitride quantum dots and edge-hydroxylated functionalization for bio-imaging. *RSC Adv.* 2016, 6, 73939–73946.
10. Cai, R.; Nie, M.; Xu, F. Ultrafast turbulence-induced disintegration of BN and WS<sub>2</sub> quantum dots for potential multifunctional nanotheranostics. *Mater. Des.* 2019, 181, 107925.
11. Zhao, H.; Ding, J.; Ji, N.; Xu, B.; Yu, H. Boron nitride quantum dots derived from renewable lignin. *ChemistrySelect* 2019, 4, 3025–3030.
12. Liu, Q.; Hu, C.; Wang, X. One-pot solvothermal synthesis of water-soluble boron nitride nanosheets and fluorescent boron nitride quantum dots. *Mater. Lett.* 2019, 234, 306–310.
13. Thangasamy, P.; Santhanam, M.; Sathish, M. Supercritical fluid facilitated disintegration of hexagonal boron nitride nanosheets to quantum dots and its application in cells imaging. *ACS Appl. Mater. Interfaces* 2016, 8, 18647–18651.
14. Angizi, S.; Hatamie, A.; Ghanbari, H.; Simchi, A.A. Mechanochemical green synthesis of exfoliated edge-functionalized boron nitride quantum dots: Application to vitamin C sensing through hybridization with gold electrodes. *ACS Appl. Mater. Interfaces* 2018, 10, 28819–28827.
15. Jerome, R.; Sundramoorthy, A.K. Hydrothermal synthesis of boron nitride quantum dots/poly(luminol) nanocomposite for selective detection of ascorbic acid. *J. Electrochem. Soc.* 2019, 166, B3017–B3024.
16. Kong, Y.; He, Y.; Zhou, J.; Zhong, S.; Song, G. Amino acids as the nitrogen source to synthesize boron nitride quantum dots for fluorescence turn-off-on detection of ascorbic acid. *ChemistrySelect* 2020, 5, 3828–3834.
17. Zhao, Y.; Butler, E.B.; Tan, M. Targeting cellular metabolism to improve cancer therapeutics. *Cell Death Dis.* 2013, 4, e532.
18. Radhakrishnan, S.; Park, J.H.; Neupane, R.; Reyes, C.A.D.L.; Sudeep, P.M.; Paulose, M.; Martí, A.A.; Tiwary, C.S.; Khabashesku, V.N.; Varghese, O.K.; et al. Fluorinated boron nitride quantum dots: A new OD material for energy conversion and detection of cellular metabolism. *Part. Part. Syst. Character.* 2019, 36, 1800346.
19. Yola, M.L.; Atar, N. Development of cardiac troponin-I biosensor based on boron nitride quantum dots including molecularly imprinted polymer. *Biosens. Bioelectron.* 2019, 126, 418–424.
20. Yola, M.L. Electrochemical activity enhancement of monodisperse boron nitride quantum dots on graphene oxide: Its application for simultaneous detection of organophosphate pesticides in real samples. *J. Mol. Liq.* 2019, 277, 50–57.
21. Peng, D.; Zhang, L.; Li, F.F.; Cui, W.R.; Liang, R.P.; Qiu, J.D. Facile and green approach to the synthesis of boron nitride quantum dots for 2,4,6-trinitrophenol sensing. *ACS Appl. Mater. Interfaces* 2018, 10, 7315–7323.
22. Peng, C.; Xing, H.; Fan, X.; Xue, Y.; Li, J.; Wang, E. Glutathione regulated inner filter effect of MnO<sub>2</sub> nanosheets on boron nitride quantum dots for sensitive assay. *Anal. Chem.* 2019, 91, 5762–5767.
23. Zhan, Y.; Yang, J.; Guo, L.; Luo, F.; Qiu, B.; Hong, G.; Lin, Z. Targets regulated formation of boron nitride quantum dots—Gold nanoparticles nanocomposites for ultrasensitive detection of acetylcholinesterase activity and its inhibitors. *Sens. Actuators B Chem.* 2019, 279, 61–68.
24. Liu, B.; Yan, S.; Song, Z.; Liu, M.; Ji, X.; Yang, W.; Liu, J. One-step synthesis of boron nitride quantum dots: Simple chemistry meets delicate nanotechnology. *Chem. A Eur. J.* 2016, 22, 18899–18907.
25. Yao, Q.; Feng, Y.; Rong, M.; He, S.; Chen, X. Determination of nickel(II) via quenching of the fluorescence of boron nitride quantum dots. *Microchim. Acta* 2017, 184, 4217–4223.
26. Han, Y.; Niu, Y.; Liu, M.; Niu, F.; Xu, Y.; Niu, F. A rational strategy to develop a boron nitride quantum dot-based molecular logic gate and fluorescent assay of alkaline phosphatase activity. *J. Mater. Chem. B* 2019, 7, 897–902.
27. Yang, K.; Jia, P.; Hou, J.; Bu, T.; Sun, X.; Liu, Y.; Wang, L. Innovative dual-emitting ratiometric fluorescence sensor for tetracyclines detection based on boron nitride quantum dots and europium ions. *ACS Sustain. Chem. Eng.* 2020, 8, 17185–17193.
28. Choudhury, S.P.; Feng, Z.; Gao, C.; Ma, X.; Zhan, J.; Jia, F. BN quantum dots decorated ZnO nanoplates sensor for enhanced detection of BTEX gases. *J. Alloys Compd.* 2020, 815, 152376.
29. Li, Q.; Zheng, Y.; Hou, X.; Yang, T.; Liang, T.; Zheng, J. A wide range photoluminescence intensity based temperature sensor developed with BN quantum dots and the photoluminescence mechanism. *Sens. Actuators B Chem.* 2020, 304, 127353.

30. Park, Y.; Koo, C.; Chen, H.Y.; Han, A.; Son, D.H. Ratiometric temperature imaging using environment insensitive luminescence of Mn-doped core shell nanocrystals. *Nanoscale* 2013, 5, 4944–4950.
31. Wang, X.; Kong, X.; Yu, Y.; Sun, Y.; Zhang, H. Effect of annealing on upconversion luminescence of ZnO:Er<sup>3+</sup> nanocrystals and high thermal sensitivity. *J. Phys. Chem. C* 2007, 111, 15119–15124.
32. Singh, S.K.; Kumar, K.; Rai, S. Er<sup>3+</sup>/Yb<sup>3+</sup> codoped Gd<sub>2</sub>O<sub>3</sub> nano-phosphor for optical thermometry. *Sens. Actuators A Phys.* 2009, 149, 16–20.
33. Wang, S.; Westcott, S.; Chen, W. Nanoparticle luminescence thermometry. *J. Phys. Chem. B* 2002, 106, 11203–11209.
34. Lan, J.; Zou, H.; Liu, Z.; Gao, M.; Chen, B.; Li, Y.; Huang, C. A visual physiological temperature sensor developed with gelatin-stabilized luminescent silver nanoclusters. *Talanta* 2015, 143, 469–473.
35. Wang, C.; Xu, Z.; Cheng, H.; Lin, H.; Humphrey, M.G.; Zhang, C. A hydrothermal route to water-stable luminescent carbon dots as nanosensors for pH and temperature. *Carbon* 2015, 82, 87–95.
36. Ding, Q.; Zhang, X.; Li, L.; Lou, X.; Xu, J.; Zhou, P.; Yan, M. Temperature dependent photoluminescence of composition tunable Zn<sub>x</sub>AgInSe quantum dots and temperature sensor application. *Opt. Express* 2017, 25, 19065–19076.
37. Chen, P.-C.; Chen, Y.-N.; Hsu, P.-C.; Shih, C.-C.; Chang, H.-T. Photoluminescent organosilane-functionalized carbon dots as temperature probes. *Chem. Commun.* 2013, 49, 1639–1641.
38. Zhai, Q.; Li, J.; Wang, E. Recent advances based on nanomaterials as electrochemiluminescence probes for the fabrication of sensors. *Chem Electro Chem* 2017, 4, 1639–1650.
39. Richter, M.M. Electrochemiluminescence. In *Optical Biosensors*; Elsevier: Amsterdam, The Netherlands, 2008; pp. 317–384. Available online: (accessed on 26 March 2021).
40. Xing, H.; Zhai, Q.; Zhang, X.; Li, J.; Wang, E. Boron nitride quantum dots as efficient coreactant for enhanced electrochemiluminescence of ruthenium(II) Tris(2,2'-Bipyridyl). *Anal. Chem.* 2018, 90, 2141–2147.
41. Qin, D.; Jiang, X.; Mo, G.; Feng, J.; Deng, B. Boron nitride quantum dots as electrochemiluminescence coreactants of @Ru–SiO<sub>2</sub> for label-free detection of AFP in human serum. *Electrochim. Acta* 2020, 335, 135621.
42. Li, M.; Wang, C.; Chen, L.; Liu, D. A novel electrochemiluminescence sensor based on resonance energy transfer system between nitrogen doped graphene quantum dots and boron nitride quantum dots for sensitive detection of folic acid. *Anal. Chim. Acta* 2019, 1090, 57–63.
43. Gao, J.; Chen, Z.; Mao, L.; Zhang, W.; Wen, W.; Zhang, X.; Wang, S. Electrochemiluminescent aptasensor based on resonance energy transfer system between CdTe quantum dots and cyanine dyes for the sensitive detection of ochratoxin A. *Talanta* 2019, 199, 178–183.
44. Chen, H.; Li, W.; Zhao, P.; Nie, Z.; Yao, S. A CdTe/CdS quantum dots amplified graphene quantum dots anodic electrochemiluminescence platform and the application for ascorbic acid detection in fruits. *Electrochim. Acta* 2015, 178, 407–413.
45. Zhang, H.-R.; Xu, J.-J.; Chen, H.-Y. Electrochemiluminescence ratiometry: A new approach to DNA biosensing. *Anal. Chem.* 2013, 85, 5321–5325.
46. Jiang, H.; Wang, X. Label free detection of folate receptor (+) cells by molecular recognition mediated electrochemiluminescence of CdTe nanoparticles. *Anal. Chem.* 2014, 86, 6872–6878.
47. Liu, Y.; Chen, X.; Wang, M.; Ma, Q. A visual electrochemiluminescence resonance energy transfer/surface plasmon coupled electrochemiluminescence nanosensor for Shiga toxin-producing Escherichia coli detection. *Green Chem.* 2018, 20, 5520–5527.
48. Liu, Y.; Wang, M.; Nie, Y.; Zhang, Q.; Ma, Q. Sulfur regulated boron nitride quantum dots electrochemiluminescence with amplified surface plasmon coupling strategy for BRAF gene detection. *Anal. Chem.* 2019, 91, 6250–6258.
49. Liang, Z.; Zhang, Q.; Nie, Y.; Zhang, X.; Ma, Q. Polarized-Electrochemiluminescence biosensor based on surface plasmon coupling strategy and fluorine doped BN quantum dots. *Anal. Chem.* 2020, 92, 9223–9229.
50. Wang, C.; Li, M.; Wang, P.; Liu, D. An electrochemiluminescence biosensor based on boron nitride quantum dots as novel coreactant for quantitative determination of concanavalin A. *Microchim. Acta* 2020, 187, 1–9.
51. Yang, Y.; Zhang, C.; Huang, D.; Zeng, G.; Huang, J.; Lai, C.; Zhou, C.; Wang, W.; Guo, H.; Xue, W.; et al. Boron nitride quantum dots decorated ultrathin porous g-C<sub>3</sub>N<sub>4</sub>: Intensified exciton dissociation and charge transfer for promoting visible-light-driven molecular oxygen activation. *Appl. Catal. B Environ.* 2019, 245, 87–99.
52. Mohanta, M.K.; Sahu, T.K.; Gogoi, D.; Peela, N.R.; Qureshi, M. Hexagonal boron nitride quantum dots as a superior hole Extractor for efficient charge separation in WO<sub>3</sub>-based photoelectrochemical water oxidation. *ACS Appl. Energy Mater.* 2019, 2, 7457–7466.

53. Sahu, T.K.; Mohanta, M.K.; Qureshi, M. Modulating water oxidation kinetics utilizing H-BN quantum dots as an efficient hole extractor on fluorine doped hematite photoanode. *J. Power Sources* 2020, 445, 227341.
54. Hu, S.; Hidalgo, M.L.; Wang, F.C.; Mishchenko, A.; Schedin, F.; Nair, R.R.; Hill, E.W.; Boukhvalov, D.W.; Katsnelson, M.I.; Dryfe, R.A.W.; et al. Proton transport through one-atom-thick crystals. *Nat. Cell Biol.* 2014, 516, 227–230.
55. Morishita, T.; Okamoto, H. Facile exfoliation and noncovalent superacid functionalization of boron nitride nanosheets and their use for highly thermally conductive and electrically insulating polymer nanocomposites. *ACS Appl. Mater. Interfaces* 2016, 8, 27064–27073.
56. Chen, J.; Huang, X.; Sun, B.; Jiang, P. Highly thermally conductive yet electrically insulating polymer/boron nitride nanosheets nanocomposite films for improved thermal management capability. *ACS Nano* 2019, 13, 337–345.
57. Wang, X.; Wu, P. Preparation of highly thermally conductive polymer composite at low filler content via a self assembly process between polystyrene microspheres and boron nitride nanosheets. *ACS Appl. Mater. Interfaces* 2016, 9, 19934–19944.
58. Chen, J.; Wei, H.; Bao, H.; Jiang, P.; Huang, X. Millefeuille inspired thermally conductive polymer nanocomposites with overlapping BN nanosheets for thermal management applications. *ACS Appl. Mater. Interfaces* 2019, 11, 31402–31410.
59. Lei, C.; Wu, K.; Wu, L.; Liu, W.; Du, R.; Chen, F.; Fu, Q. Phase change material with anisotropically high thermal conductivity and excellent shape stability due to its robust cellulose/BNNSs skeleton. *J. Mater. Chem. A* 2019, 7, 19364–19373.
60. Han, J.; Du, G.; Gao, W.; Bai, H. An anisotropically high thermal conductive boron nitride/epoxy composite based on nature-mimetic 3D network. *Adv. Funct. Mater.* 2019, 29, 1900412.
61. Wang, T.; Wang, M.; Fu, L.; Duan, Z.; Chen, Y.; Hou, X.; Wu, Y.; Li, S.; Guo, L.; Kang, R.; et al. Enhanced thermal conductivity of polyimide composites with boron nitride nanosheets. *Sci. Rep.* 2018, 8, 1–8.
62. Yuan, J.; Qian, X.; Meng, Z.; Yang, B.; Liu, Z.-Q. Highly thermally conducting polymer based films with magnetic field assisted vertically aligned hexagonal boron nitride for flexible electronic encapsulation. *ACS Appl. Mater. Interfaces* 2019, 11, 17915–17924.
63. Pan, C.; Long, M.; He, J. Enhanced thermoelectric properties in boron nitride quantum-dot. *Results Phys.* 2017, 7, 1487–1491.
64. Zhou, S.; Xu, T.; Jiang, F.; Song, N.; Shi, L.; Ding, P. High thermal conductivity property of polyamide imide/boron nitride composite films by doping boron nitride quantum dots. *J. Mater. Chem. C* 2019, 7, 13896–13903.
65. Beytur, M. Fabrication of platinum nanoparticle/boron nitride quantum dots/6-methyl-2-(3hydroxy-4-methoxybenzylidene amino)-benzothiazole (IIs) nanocomposite for electrocatalytic oxidation of methanol. *J. Chil. Chem. Soc.* 2020, 65, 4929–4933.

---

Retrieved from <https://encyclopedia.pub/entry/history/show/19903>